Baroclinic Flow and Transient-Tracer Fields in the Canary–Cape Verde Basin

GERHARD THIELE,* WOLFGANG ROETHER, PETER SCHLOSSER AND REINHARD KUNTZ

Institut für Umweltphysik, University of Heidelberg, 6900 Heidelberg, F.R.G.

GEROLD SIEDLER AND LOTHAR STRAMMA

Institut für Meereskunde, University of Kiel, 2300 Kiel, F.R.G.

(Manuscript received 8 April 1985, in final form 13 September 1985)

ABSTRACT

Simulated transient-tracer distributions (tritium, ^{3}He, freons) on the isopycnal horizons σ_θ = 26.5 and 26.8 kg m^{-3} are presented for the East Atlantic, 10°–40°N. Tracer transport is modeled by employing a baroclinic flow field based on empirical data in a kinematic isopycnal advection-diffusion numerical model, in which winter convection is taken as the mechanism of communication with the ocean surface layer, and the isopycnal diffusivity is a free parameter. Diapycnic transport is ignored. The simulations employ time-dependent tracer boundary conditions, which are constructed on the basis of available observations. Simulations are compared to data obtained on a meridional section in 1981 (F/S *Meteor*, cruise 56/5). Best simulations were obtained by means of a subjective optimization procedure. On both levels, the observed distributions and the best simulated distributions agree well. The fact that the surface boundary conditions and interior distributions of the tracers are distinctly different leads us to the conclusion that our model provides a consistent description of upper main-thermocline ventilation and interior transport. Surface-water densities in February are found to represent adequately the winter outcrop boundaries, with an uncertainty of about ±300 km across. The required isopycnal diffusivity south of 29°N is 1700 m^2 s^{-1}, and 2900 m^2 s^{-1} further north (+70/−40%). Interior transport is found to be predominantly advective. Advective ventilation across 30.5°N east of 33°W amounts to only 12% and 40% for the 26.5 and 26.8 horizons of the total ventilation rates reported by Sarmiento. The North Atlantic/South Atlantic Central Water boundary near 15°N is found to be predominantly determined by advection.

1. Introduction

The internal recirculation of North Atlantic main thermocline water and its interfacing with the ocean surface layer (ventilation) have been the subject of a number of recent publications (McCartney, 1982; McDowell et al., 1982; Luyten et al., 1983a,b; Cox and Bryan, 1984). Much of the work was oriented toward understanding the flow dynamics with emphasis on potential vorticity conservation. The usefulness of transient tracer observations in this context has been shown by Sarmiento et al. (1982) on the basis of a 1972–73 tritium survey. Because these tracers have been added to ocean surface waters in a distinct areal and time pattern, their subsequent appearance in the ocean interior will reflect the exchange with the ocean surface layer in a quantifiable way. The discussion by Sarmiento et al. (1982) at least demonstrated a qualitative correspondence between the observed tritium field and the water mass distribution expected according to main thermocline ventilation models.

Ventilation implies exchanges of matter and heat between the ocean surface layer and the interior and is thus of climatological, geochemical and environmental relevance. Ocean models have been formulated to quantify this exchange (Cox and Bryan, 1984). Transient-tracer data are attractive in this context because oceanic tracer transport is fully analogous to the transport of other dissolved substances, and essentially also to that of heat, and because they contain information on typical time scales of some years where other observational evidence is scarce. However, it is clear that in order to exploit fully the potential of the tracer data appropriate ocean models are required (Sarmiento, 1983a).

The quantitative modeling of tracer distributions taking account of main thermocline ventilation is not well advanced at the present time. A very simple gross-transfer approach of ocean surface/ocean interior exchange for the North Atlantic was used by Weiss et al. (1979), and Sarmiento (1983b) calculated, on the basis of the tritium dataset already mentioned, the bulk exchange rates for the main thermocline waters using an isopycnal box model. It is attempted here to proceed further along this line by providing a more explicit formulation of the water mass transport. Model simulations for the density horizons σ_θ = 26.5 and 26.8 are compared to simultaneous observations for the tran-

* Present address: Princeton University, Princeton, NJ 08540.

sient tracers tritium, tritiugenic ^{3}He, and the freons. These tracers have distinctly different distributions, the tritium/^{3}He pair specifically allowing one to deduce interior-ocean travel times. The combination of these tracers, therefore, will subject the model to particularly powerful constraints. The analysis represents a further step in developing the methodology for inverting transient tracer observations into oceanic transport information.

The following section includes an assessment of recent results on surface layer to interior transfers and the interior circulation field. Subsequently, the observational data are described that were obtained on a long meridional section in the northeast Atlantic with F/S *Meteor* in 1981, and ocean-surface tracer boundary conditions are presented. Following a model description in section 4, model-simulated tracer distributions are compared to the observational data.

2. Surface transfer and interior circulation

Water distribution in the main thermocline is usually pictured as being the result of vertical processes at higher latitudes generating distinct water masses, and isopycnal baroclinic flow and predominantly isopycnal mixing of these water masses at greater depths and lower latitudes. It is now well established (Sarmiento et al., 1982) that the transfers between the ocean surface layer and the interior circulation are dominated by late-winter overturning ("winter convection") implying a change in potential vorticity. In the interior of the eastern subtropical gyre, however, the flow can be assumed to be potential vorticity conserving, with the current field being aligned with lines of constant potential vorticity (Luyten et al., 1983a). This constraint leads to a subtropical gyre with particularly slow water renewal in the SE part of the North Atlantic (Fig. 1).

Based on this concept, the following approach is used here: Winter surface water characteristics are imposed wherever the respective isopycnal surface is reached by winter convection. The interior flow is assumed to be entirely isopycnal and is separated into mean flow and

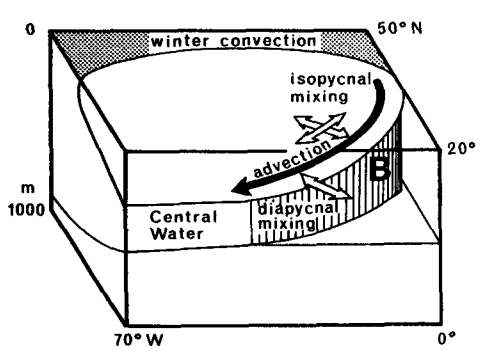

FIG. 1. Schematic presentation of winter convection area and the ventilated and unventilated regions with their boundary B (see also Luyten et al., 1983b, Fig. 8).

time-dependent components, the latter being described by an apparent eddy diffusivity. Diapycnal mixing is neglected in the interior (Armi, 1978; Armi and Stommel, 1983). This leads to two-dimensional flow patterns on isopycnal surfaces.

The mean flow is obtained from 3° × 3°-square averaged historical hydrographic data (Siedler and Stramma, 1983). For the later selection of the two density surfaces, σ_θ = 26.5 and 26.8 kg m^{-3}, the actual choice of the level-of-no-motion is not critical because of the shallowness of those density surfaces (Stramma, 1984); a zero-level of 1200 db was selected. Geopotential anomalies were smoothed, using double Chebychev polynominals of third order on pressure levels 0, 200, 350 and 500 db. The two density surfaces were smoothed correspondingly, and geostrophic velocities were linearly interpolated to obtain their values on the two density surfaces given above.

The resulting flow fields are presented in Fig. 2. The results are consistent with the currents that were obtained from β-spiral calculations by Behringer (1979) and Behringer and Stommel (1980) in the central part of the area under discussion (indicated in Fig. 2 by B, BS). It should be noted, however, that the heavy smoothing masks a dominating feature of the flow field near the Azores where the major portion of the eastern Atlantic subtropical gyre recirculation is found in a frontal jet (Käse and Siedler, 1982; Käse et al., 1985; Siedler et al., 1985). Moreover, the data handling procedure leaves gaps in the velocity field near the African coast.

Winter outcrop areas of specified isopycnal surfaces are obtained by identifying the seasonal maximum southward displacement of that density in surface waters. Estimates of these boundaries are available for the North Atlantic (U.S. Naval Oceanographic Office, 1967; Robinson et al., 1979; Levitus, 1982; Gorshkov, 1978). Their application for the present purpose is not straightforward because of the effects of data averaging and interannual variability. Details are given in section 4.

Apparent isopycnal eddy diffusivity estimates for the southern part of our investigation area (Fig. 2) are available from the β-triangle data analysis of Armi and Stommel (1983). The estimates were obtained by balancing advective flux divergencies for salinity and oxygen against diffusive ones. The authors report $K \approx 500$ m^2 s^{-1} below σ_θ = 27.1, with a tendency toward larger values above this density level. Still somewhat larger values can be expected further north, owing to enhanced eddy kinetic energy density that is observed there (Käse et al., 1985), being related to the jet previously mentioned.

3. Tracer observations and ocean-surface tracer boundary conditions

The principal dataset consists of tritium, ^{3}He, and freon measurements on water samples obtained at sta-

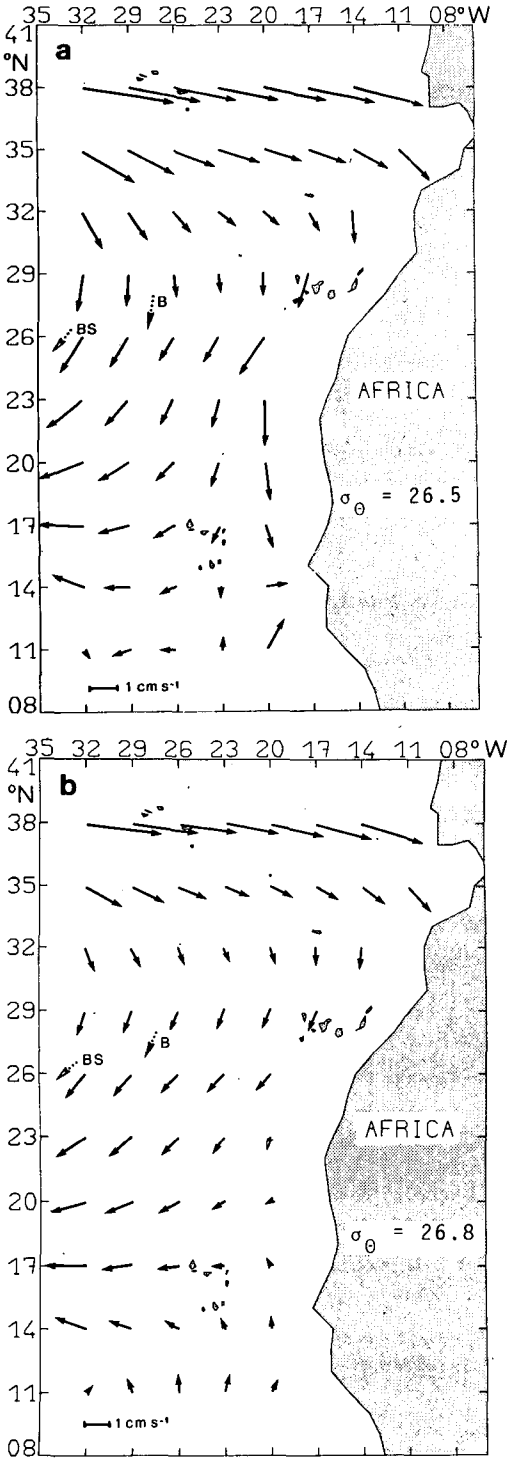

FIG. 2. Velocity vectors on (a) the 26.5 and (b) the 26.8 potential-density horizon; for explanation see text.

tions along a meridional section, 8°S–46°N, in the eastern Atlantic, carried out during cruise 56, leg 5, of the F/S *Meteor*, in March–April 1981. Tritium and ^{3}He samples were collected and stored using standard procedures (Weiss et al., 1976; Weiss, 1968), and sample validity was checked on the basis of consistency of hydrographic data (Schlitzer et al., 1985) that were obtained together with the tracer data. Tritium measurements were carried out at Heidelberg by gas counting, using procedures described previously (Weiss et al., 1976), and are reported as tritium ratios (TR) on the scale proposed by Taylor and Roether (1982) (TR, synonymous to TU, means a 10^{-18} [T]/[H] ratio). Precision usually is ±5% or TR = ±0.08, whichever is greater, and a systematic bias in the lowest measured concentrations is believed to be less than TR = 0.05. Concentrations of ^{3}He were measured by mass spectrometry (Clarke et al., 1976), with the Heidelberg ^{3}He-facility, and are reported as deviations from the atmospheric concentration ratio R_{air} = [^{3}He]/[^{4}He], δ^3He = $(R_{sample} - R_{air})/R_{air} \times 100\%$. Measuring precision of δ^3He is ±0.2% or better. Some samples were lost because of incomplete He extraction in the sample processing procedure.

Freon samples (~0.4 L) were collected in 5-L stainless-steel Niskin-type samplers and were placed for storage into preevacuated, pretreated stainless-steel containers using a special filling device designed to minimize contact with, and inclusion of, ambient air. For measurement of the freon-11 and freon-12 (F-11, F-12) concentration at Heidelberg, the contained gas was released from the containers and transferred via a collection trap into a gas chromatograph equipped with an ECD detector (Perkin-Elmer). Data are reported in pmol/kg. Data precision is estimated to be generally ±5%. However, internal calibration inconsistencies of the same magnitude cannot be excluded for part of the data, and some erroneously high values had to be eliminated. Data blanks were assessed from results for water regarded as essentially freon-free on the basis of the tritium results, and they amount to ⩽5% of the surface water freon concentrations. The reported data are corrected for these blanks (F-11: 0.07 ± 0.01; F-12: 0.03 ± 0.01 pmol/kg). Our freon calibration is linked to that of the KFA Jülich tracer gas laboratory, which is supposed (J. Rudolph, private communication, 1984) to be 3–5% lower than that for other oceanic and for atmospheric freon data reported in the literature (Gammon et al., 1982; Bullister and Weiss, 1983; Cunnold et al., 1983a,b).

Figure 3 indicates the location of the *Meteor* 1981 stations. For these stations, tracer concentrations on isopycnal surfaces were estimated by subjective interpolation of tracer-concentration versus σ_θ plots. Tritium concentrations on various isopycnals along the *Meteor* section obtained in this way, as well as in surface water, are shown in Fig. 4. They exhibit a general north to south decrease on all horizons, with some secondary structure being indicated, such as a relative tritium minimum near 30°N for the σ_θ = 26.5 and 26.8 layers. The concentrated tritium decline centered around 15°N for the shallower density horizons (26.5 and 26.8)

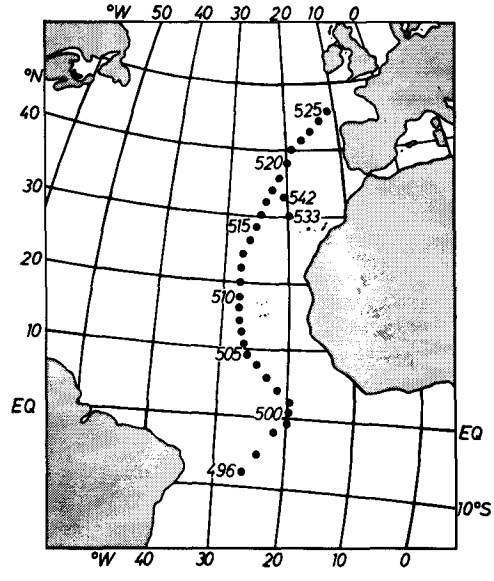

FIG. 3. Track and stations (496–525) of cruise 56, leg 5 of the F/S *Meteor*, March–April 1981, from which our present transient-tracer data originate. Stations 533 and 542 stem from cruise 57, leg 1 of the F/S *Meteor* in July 1981.

marks the boundary between the North Atlantic and South Atlantic Central Waters (NACW, SACW; Worthington, 1976). For the deepest horizon shown (27.1), the tritium decline is shifted northward and is more gradual. The pronounced north–south tritium asymmetry primarily results from less tritium having been delivered to the Southern Hemisphere ocean (Weiss and Roether, 1980). However, the longer travel distance from the outcrop areas for the SACW part of the section presumably reinforces the asymmetry. Apart from shallow-depth inversions, the tritium concentrations decrease downward, and they are essentially zero south of 10°N on the σ_θ = 27.1 horizon. Owing to data limitations, the distributions for ^{3}He and the freons are documented in less detail than for tritium, but well enough that the differences in the distributions of the tracers become manifest. Generally speaking, the north–south asymmetry for the freons is less than for tritium (because only a small interhemispheric freon gradient in the atmosphere, and hence in surface water, exists). There is, contrary to tritium, a marked north to south freon decline within the NACW part of the section also for the density horizons σ_θ = 26.5 and 26.8. For these same layers, ^{3}He attains maximum values on the northern side of the Central Water boundary, and it decreases in concentration toward solubility equilibrium values with the atmosphere toward the outcrops.

Errors of the isopycnal tracer concentrations were also estimated on the basis of the analytical errors of the data on which the interpolation was actually based, and, if necessary, additionally accounting for an uncertainty of the interpolation. The latter contribution is particularly large for ^{3}He, for which the density horizons in question (26.5 and 26.8) fall into a depth range of pronounced vertical concentration gradients, and the estimated total errors often greatly exceed the actual measurement errors. The model evaluation below also uses some freon concentrations based on data from *Meteor* cruise 57, 1981.

Tritium is predominantly, and the freons are fully, manmade, and all have been delivered to the ocean surface during the last few decades. Figure 5 gives surface-water concentration histories for the midlatitude North Atlantic, 1952–82. Tritium (Dreisigacker and Roether, 1978) went through a maximum in about 1965 whereafter it gradually decreased, faster than by radioactive decay alone, while freon concentrations have been rising steadily. This difference explains the mentioned observation that tritium is more uniformly distributed in the ocean interior than are the freons. Tritium concentrations in ocean surface water can be factorized into time (see Fig. 5) and areal distribution functions. As for the latter, the survey of Dreisigacker and Roether (1978) indicated surface-water concentrations to be essentially constant areally north of a tritium decline zone centered around 20°N, whereas Fig. 4 shows a two-step decline to have existed along the 1981 *Meteor* section, the northern step amounting to about 20% in concentration and being centered near 35°N. A north–south decline starting well north of 20°N is also indicated in 1973 surface-water concentrations, presented in Fig. 6. The limited evidence available thus indicates the southward tritium decline to be structured, with perhaps even a time trend in the actual pattern. A latitudinal pattern corresponding to Fig. 4 is used for the model evaluation below. Uncertainties remain, however, because of data scatter and insufficient areal coverage in the observations.

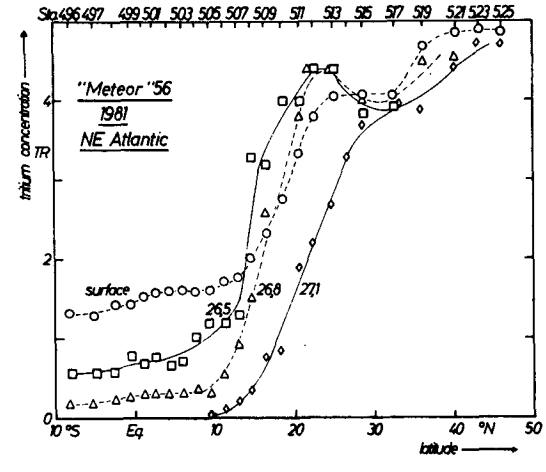

FIG. 4. Tritium concentrations in surface water and on various isopycnal surfaces (figures at curves indicate σ_θ) for the 1981 *Meteor* section. For explanation see text; for concentration uncertainties see Figs. 8–11.

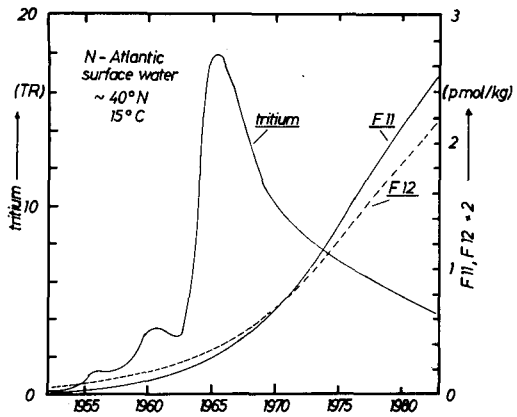

FIG. 5. Surface-water tritium and freon time histories, North Atlantic ~40°N *Tritium:* 1952–75 from Dreisigacker and Roether (1978), 1975–82 geometrically interpolated to meet the observed 1981 value (Fig. 4). *Freon:* Assuming solubility equilibrium (15°C) with atmospheric concentrations (see text).

Freon concentrations in surface water are more easily assessed in principle, as they can be assumed to be near to a solubility equilibrium with atmospheric concentrations. Extensive atmospheric freon measurements are available since 1979 (Cunnold et al., 1983a,b). Earlier concentrations were obtained by fitting the accumulated atmospheric freon releases (Battelle, 1976; Cunnold et al., 1983a,b) to these measurements (the freons were assumed to be inert in the atmosphere, which should be adequate for our purpose). Solubilities reported recently (Wisegarver and Cline, 1985; Warner and Weiss, 1985) agree within a few percent. Wisegarver and Cline checked their solubilities against measured surface water concentrations and found considerable scatter but no bias, whereas our own surface water measurements, using the same solubilities, do indicate an apparent undersaturation of about 5% for both freons. The model simulations below will use surface water concentrations calculated from atmospheric concentrations and the Warner and Weiss (1985) solubilities. On the basis of the mentioned bias and of our measurement calibration, we conclude that, relative to our measured data, the F-11 simulations might be high by 10 ± 5%, and the F-12 ones by 5 ± 5%.

Concentrations of ^{3}He in surface water can be assumed to be essentially constant, by attaining a solubility near-equilibrium with atmospheric helium (for details see Fuchs et al., 1986). A value of $\delta^3\text{He} = -1.4\%$, based on observational data, is used below. This value is slightly in excess of the true equilibrium value (Benson and Krause, 1980), and its uncertainty should be no larger than ±0.25%. In the interior a tritiugenic ^{3}He excess grows in from tritium decay. The ±0.25% uncertainty translates into a tritium/^{3}He "age" uncertainty of approximately ±0.3 years.

The model outlined in the next section applies the time-dependent tracer surface boundary conditions described here and integrates tracer transport in the interior in time over the entire period since tritium and the freons have appeared in ocean surface waters. Initial concentrations are zero for the freons and negligibly small for tritium in view also of tritium decay (Dreisigacker and Roether, 1978). For ^{3}He, a small excess initial concentration (1%) has to be accounted for, which results from the decay of natural tritium (Dreisigacker and Roether, 1978) and from terrigenic ^{3}He being admixed from the South Atlantic (Jenkins and Clarke, 1976).

4. The model

The model to simulate the isopycnal tracer distributions is a two-dimensional, time-dependent kinematic multibox model, in which the equation of continuity for the tracer,

$$\frac{\partial c}{\partial t} = -\mathbf{u}\cdot\nabla c + K\cdot\Delta c - \lambda\cdot c + S \qquad (1)$$

is integrated numerically. Here, $c(\mathbf{x}, t)$ = tracer concentration, $\mathbf{x}$ = position vector, t = time, $\mathbf{u}(\mathbf{x})$ = two-dimensional time-averaged isopycnal velocity vector, $K(\mathbf{x})$ = apparent isopycnal diffusivity, λ = decay constant (for tritium), and S = source term for ^{3}He $= \lambda\cdot c_{\text{tritium}}$. The freons are regarded as conservative ($\lambda_{\text{freon}} = S_{\text{freon}} = 0$). The model geometry follows Fig. 2. Boxes of 3° × 3° size are centered around the origins of the arrows in the figure. Velocity components normal to the boundaries of these boxes are available from the velocity-field computation procedure (see section 2). Compared to Fig. 2, the model has some additional boxes next to the coast, to the extent that through the procedure at least one in- and one outflow are defined for any such box. The original velocity field has nonvanishing divergence, particularly so in the zone of extensive eastward flow near 36°N. The actual divergence there appears to be consistent with a notion that part of the flow enters the Mediterranean or is removed

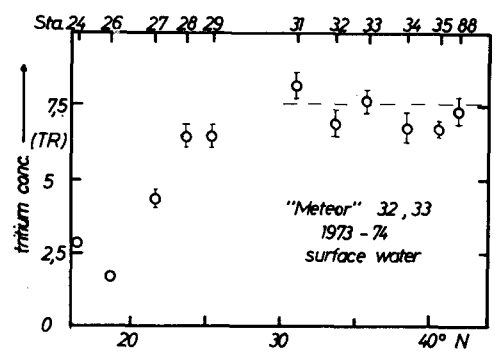

FIG. 6. Surface-water tritium versus latitude for *Meteor* cruise 32, Nov–Dec 1973 (Stas. 24–35), and 33, March 1974 (Sta. 88): error bars are analytical errors, dashed line is value according to Fig. 5.

into deeper water by being entrained into the Mediterranean outflow (Worthington, 1976). On this reasoning, the velocity field was readjusted divergence-free by a least-squares procedure (Lawson and Hanson, 1974), allowing for a Mediterranean sink. The sink was varied such that changes in the original field south of 30.5°N were minimized; the implied velocity changes there are typically within ±5%, ensuring that the basic features of the original velocity field are unchanged.

The isopycnal diffusivity K is taken as a free parameter in the model. It is allowed to be different south and north of 29°N (K_S, K_N) in order to account for the expected northward increase (section 2), but it is taken as constant within each subdomain.

Surface-water tracer concentrations are imposed north of the late-winter outcrop boundary for the respective density level. In the model calculations this condition is applied throughout the year, despite the fact that the actual outcropping is seasonally restricted. As density in the interior, for the area and densities under consideration, is sufficiently well related to temperature (Siedler and Stramma, 1983), the outcrop boundaries were taken from the monthly mean temperature maps given by Robinson et al. (1979). Specifically, they were identified with the position of the appropriate temperature isoline in the February map (which represents seasonal-minimum conditions) for 30 m depth. The temperatures chosen were those that coincide with the potential temperatures on the selected density levels along the *Meteor* section (σ_θ = 26.5: 18.5°C; 26.8: 15°C). The alongsection variation in the σ_θ-temperature relationship appears to amount to about ±0.3°C. The temperature map gives the corresponding uncertainty in the position of the boundary as generally no more than 100 km, or appreciably smaller than the box dimensions. Other available outcrop information (U.S. Naval Oceanogr. Office, 1967; Gorshkov, 1978; Sarmiento et al., 1982) places the boundaries somewhat differently; in the case of the Sarmiento et al. (1982) outcrops this is due to winter season average data having been used, while we use monthly mean seasonal minimal data.

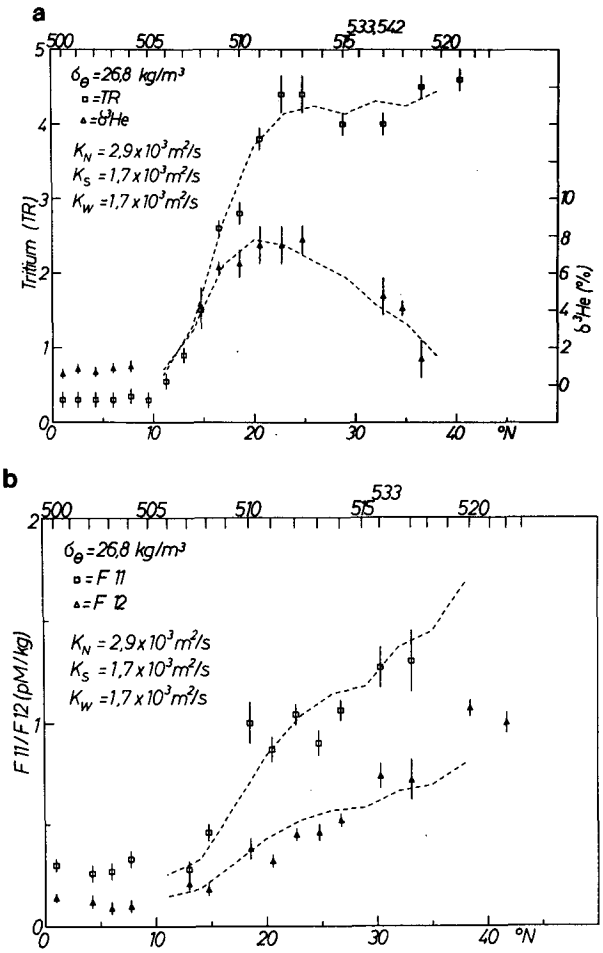

FIG. 8. Optimum simulated and observed tracer concentrations on the σ_θ = 26.8 level along the 1981 *Meteor* track, diffusivity values K_S = 1700 m² s⁻¹, K_N = 2900 m² s⁻¹, K_W = 1700 m² s⁻¹. For each station for which a meaningful tracer concentration can be obtained, the value and its error margin are given. (a) Tritium and ³He (b) Freon-11 and Freon-12.

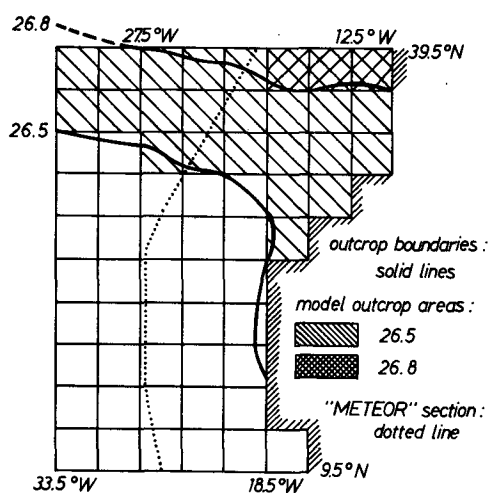

FIG. 7. Model geometry, boundaries of winter convection, model outcrop areas and position of *Meteor* 56/5 section.

The σ_θ = 26.5 and 26.8 outcrop boundaries according to our choice, as well as their representation within the resolution of our model, are shown in Fig. 7. On both density horizons, the boundaries fall within, or at least border, the model area, so that the procedure just outlined defines a northern tracer boundary condition for the model.

For defining a southern tracer boundary condition, observed tracer concentrations are available only for 1981 (Figs. 4, 8, 9) whereas concentrations prior to 1981 have to be estimated. It is evident, however, that in 1981 tracer concentrations south of the Central Water boundary were still quite small, so that the actual

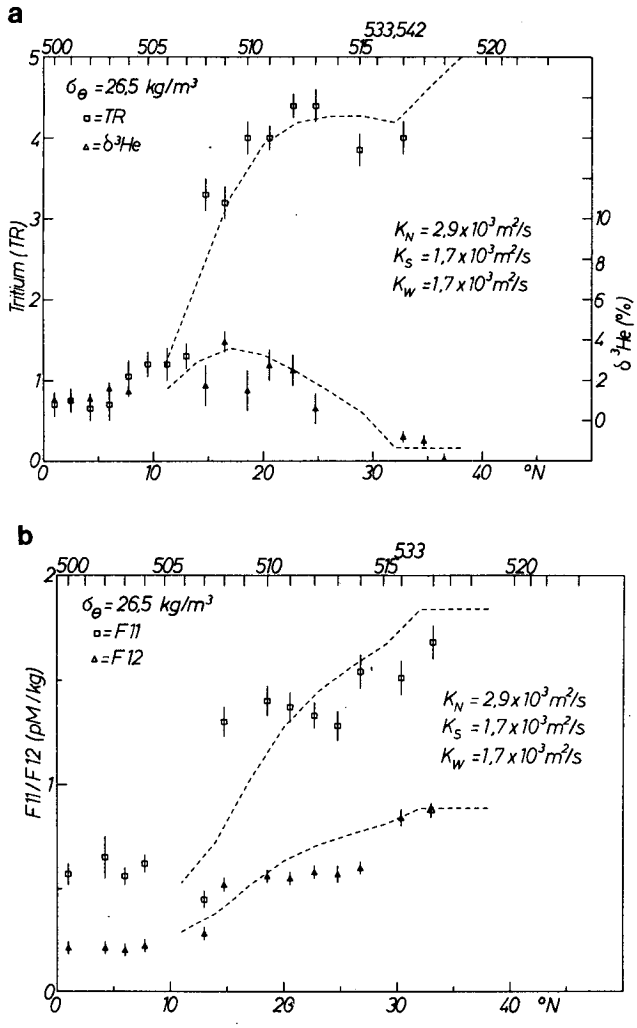

FIG. 9. Tracer concentrations on the $\sigma_\theta = 26.5$ level; for details see Fig. 8.

southern tracer boundary condition should be rather uncritical. Being located south of the Central Water boundary, the southern model boundary should receive its tracer imprint primarily from the South Atlantic outcrop areas of the two density levels. South Atlantic surface-water concentrations (tritium: data from Fig. 5 renormalized by Northern-to-Southern Hemisphere tritium-deposition ratio after Weiss and Roether, 1980; freons: procedure as for Fig. 5) were therefore applied to one end of an ad hoc delay model. The model consists of a series of 5 boxes, the exchange rates between the boxes being adjusted to reproduce simultaneously, in the far-end box, the observed 1981 tritium and freon concentrations on the southern model boundary. It was found that some admixture of Northern Hemisphere surface water to the far-end box had to be allowed for (exchange time scale: 80 years; see section 6), because the observed 1981 tritium-to-freon ratio could not be reproduced otherwise.

More critical is a western tracer boundary condition for the isopycnals in question, which is required north of 30.5°N, where there is flow eastward into the model area (Fig. 2), insofar as the concentrations are not imposed by winter convection (Fig. 7). The actual upstream trajectories of this flow are unknown, but dynamical-model results of Sarmiento and Bryan (1982) indicate them to run approximately parallel to the outcrop boundaries for 1000 km or more. Part or all of the trajectories might possibly be ventilated, but to the extent that this is not the case one would expect tracer to be added to the flow by across-flow isopycnal mixing from the outcrops. It is furthermore evident from the isopycnal tritium maps presented by Sarmiento et al. (1982) that, whatever the actual process of tracer addition, the upstream tritium concentrations are almost as large as those in surface water. The boundary condition in question was therefore constructed by closing the circulation through the model area by an ad hoc divergence-free recirculation to the west (to represent, in a way, the gyre recirculation) and letting tracer be recirculated with this flow, but primarily letting it be added by lateral diffusion from the winter-convection boundary to the north of the ad hoc recirculation domain. The westward recirculation essentially extends our derived flow velocities normal to and across 33.5°W (section 2, Fig. 2) and outcrop boundaries at this longitude (Fig. 7) zonally to the west, over a distance of about 2500 km. It is thus over such distance that diffusive tracer intrusion from the outcrop is allowed for. The corresponding isopycnal diffusivity (K_w) is a free ad hoc parameter in the model calculations. It is to be noted again that because the tracer concentrations are fairly close to the surface water values, only the actual degree of concentration deficiency has to be modeled.

The numerical formulation of the advection uses an upwind difference scheme (Roache, 1972). Tests were run with an implemented Fiadeiro and Veronis (1977) weighted-mean difference scheme, which, however, gave only minor differences in the results, presumably because our transports are predominantly advective. Box thickness is uniform in our model, but thicknesses proportional to $(\partial\sigma/\partial z)^{-1}$ have also been tested ($z \equiv$ vertical coordinate), again with results being insignificantly changed. Similarly, the velocity field was modified to allow part of the eastward flow north of 30.5°N to be concentrated meridionally in order to artificially form the jet that is observed there, but is not resolved in the present velocity field (see section 2).

Numerical integration of Eq. (1), with initial and boundary conditions for the tracers, was done with an explicit algorithm (Roache, 1972). A time step of 0.03 years was used, which was verified to be within the range of numerical stability of the algorithm. Calculations have been carried out on an IBM 3081D computer, at less than 10 s CPU-time per run. Simulated

tracer concentrations for the appropriate time step were interpolated to the position of the *Meteor* 1981 section, which section is also shown in Fig. 7, in order to be compared to the observations. The free parameters of the model (see Table 1) were varied systematically, and, for quick reference, a mean as well as a mean-square deviation between simulated and observed tracer concentrations were calculated for each run.

5. Model results

The diffusivities were varied over the ranges shown in Table 1, and the resulting model runs searched for best simulation of the tracer observations. The procedure involved both inspecting the mean-square model/data deviations (Quay et al., 1983) and comparing model and observed distributions. The ad hoc diffusivity K_W, as expected, was found to be of little influence for the shallow horizon (see section 4). On the deeper horizon, on the other hand, it is clear that both K_W and K_N act to bring tritium and freons southward from the outcrop boundary, so that one diffusivity could to some extent substitute the other. This expectation is in fact borne out in the mean-square model/data deviation values. It turns out, however, that for ^{3}He the allowed $K_N - K_W$ combinations are different. This arises because, if tritium is admixed to a mean-flow trajectory early on (K_W large and K_N correspondingly smaller), more time for ^{3}He ingrowth becomes available. The procedure consistently pointed to diffusivities $K_S = 1700$ m^2 s^{-1}, $K_N = 2900$ m^2 s^{-1}, $K_W = 1700$ m^2 s^{-1} as optimum parameter values, in accordance with both the positions of the mean-square deviation minima in $K_S/K_N/K_W$ space and the distributions, and being valid for both horizons. The uncertainties of these diffusivities according to the procedure appeared to be approximately +70/−40%, i.e., a change by a factor of 1.7 in both directions.

The simulations corresponding to this set of diffusivities are shown in Figs. 8 and 9. One finds a general agreement between simulations and observational data within the data uncertainties (one-sigma errors are shown). Exceptions are the only partially reproduced tritium minimum in 30° to 35°N on both horizons, and a low simulation for the data of Sta. 508, in 14.75°N, on the $\sigma_\theta = 26.5$ horizon. In view of the freon calibration uncertainties and the possibility of some high values that were pointed out in section 3, the somewhat larger scatter in the freon data, relative to the simulated freon distributions, is not surprising. The high tracer concentrations on Sta. 508 in Fig. 9 are expected, because here untypically salty water, i.e., a strong NACW component, was met. Obviously, a mesoscale feature has been encountered, which naturally is not resolved in our model.

The effect of the uncertainty ranges of K_S and K_N (see above) is demonstrated for the 26.8 horizon in Figs. 10 and 11. The simulated distributions respond to these variations quite individually for each of the tracers. In Fig. 10, for example, in which K_S, the diffusivity south of 29°N, is varied, the effect is considerably stronger on ^{3}He and tritium than on the freons. The reason is that the latitudinal variation south of 29°N has more curvature for ^{3}He and tritium than for the freons. For a variation of K_N (Fig. 11), on the other hand, the effect on ^{3}He is less than for tritium and the freons. This occurs because the latter depend on diffusive transport to bring adequate amounts of tracer southward from the outcrops, whereas for ^{3}He a changed tritium concentration and corresponding change in diffusive ^{3}He loss to the outcrop counteract one another.

The fact that the simulated ^{3}He distributions in the latitudinal range of ^{3}He declining north of the maximum are only moderately affected by changes in the diffusivities, allows one to place limits on the effective outcrop boundaries. This holds because given the isopycnal velocity field a latitudinal shift in the boundaries to first order should induce a similar shift in the

TABLE 1. Summary of model features.

Feature	Values or reference in text	Parameter, variation range
Model area	9.5° to 39.5°N, African coast to 33.5°N	—
Model geometry	Fig. 7, 63 boxes à 3° × 3°, uniform thickness	—
Isopycnal horizons run	$\sigma_\theta = 26.5$ and 26.8	—
Isopycnal velocity field	Fig. 2a, b, modified to be divergence-free, section 4	—
Winter outcrop boundaries	Fig. 7, section 4	—
Initial and time-dependent surface and northern boundary conditions for tracers	Section 3; Fig. 5	—
Southern model boundary condition for tracers	Section 4	—
Western model boundary condition for tracers	Section 4	ad-hoc diffusivity $K_W = 500 \cdots 5000$ m^2 s^{-1}
Isopycnal diffusivity <29°N	—	$K_S = 100 \cdots 5000$ m^2 s^{-1}
Same, >29°N	—	$K_N = 500 \cdots 8500$ m^2 s^{-1}
Integration period, tritium/^{3}He	1952 to year of observation	—
Same, freons	1933 to year of observation	—

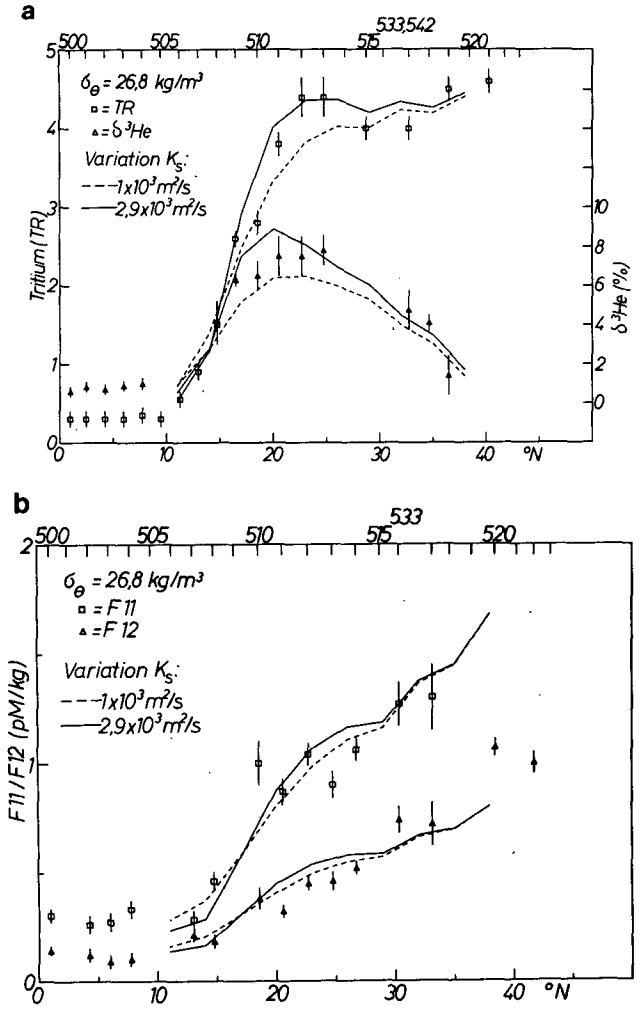

FIG. 10. Tracer concentrations on the σ_θ = 26.8 level, with K_S varied. Curves are shown for K_S = 1000 (dashed line) and 2900 m^2 s^{-1} (solid line), equivalent to a variation of a factor of 1.7 in both directions from value in Fig. 8; for details see Fig. 8.

simulated ^{3}He decline. Maintaining that a shift amounting to at most ±1% on the ^{3}He axis would be consistent with the data, and projecting this uncertainty on the latitudinal axis, one obtains a latitudinal uncertainty of the outcrop boundary of approximately ±3°, equivalent to the linear box dimensions in our model.

Whereas for the σ_θ = 26.8 horizon the evidence compiled in section 3 pointed to areally uniform surface-water tritium concentrations in the vicinity of the outcrops, this was not the case for the 26.5 horizon. Therefore, the tritium simulations for the latter horizon are subject to the uncertainties in the surface water tritium pattern. As for the possible time dependence of this pattern, however, it is noted that whereas the simulated tracer distributions were obtained by model integration over a period of some decades (Table 1), the actual tracer transit time through the model area is a smaller fraction of this period only. Therefore, the tracer boundary conditions more than some years prior to observation have little effect on the simulated distributions and are thus uncritical.

The relative tritium maximum that appears in the data near 23°N (Figs. 8 and 9) is interpreted as resulting from water subducted from the outcrops earlier in time than the water farther north and hence containing more tritium according to the general surface-water tritium concentration decline with time (Fig. 5, corrected for tritium decay). The adjoining relative minimum near 30°N for the 26.5 horizon is believed to be caused by a projection of the latitudinal surface-water tritium pattern along the outcrop (Fig. 7) into the interior by the flow trajectories. For the deeper horizon, on the other hand, our explanation is to ascribe it to a north–south tritium concentration decrease across the zonal inflow of water north of 30.5°N into the model area (Fig. 2), as a result of increasing across-stream, or pos-

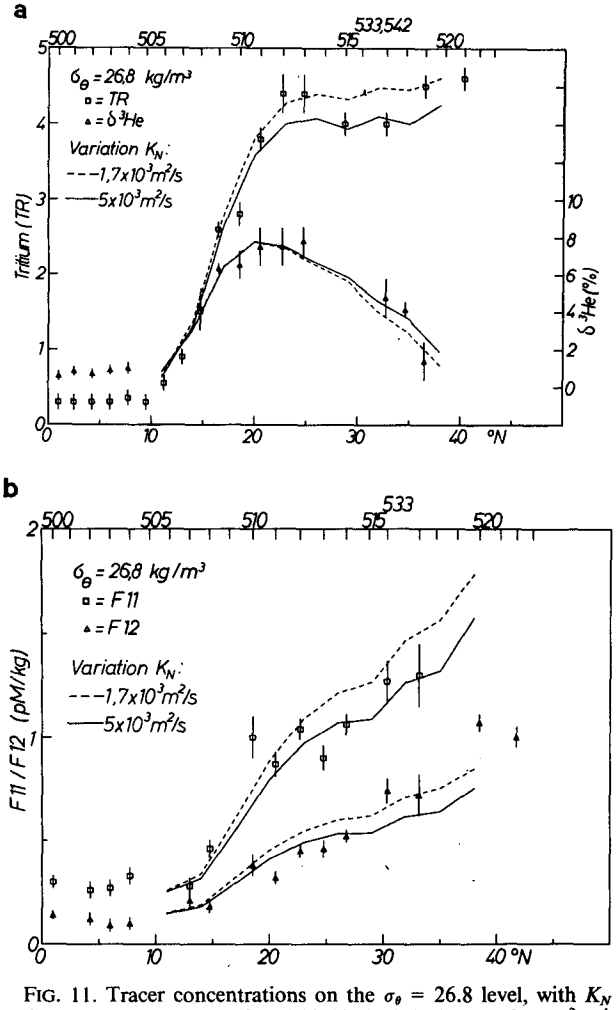

FIG. 11. Tracer concentrations on the σ_θ = 26.8 level, with K_N varied. Curves are shown for 1700 (dashed line) and 5000 m^2 s^{-1} (solid line); for details see Fig. 8.

sibly upstream, distance from the outcrop boundary for the layer.

To summarize, we believe that the model simulations reproduce the observed tracer distributions in a very satisfactory manner, the degree of agreement being somewhat less for the $\sigma_\theta = 26.5$ horizon. As for testing the model in detail, such as concerning the tritium extrema mentioned in the preceding paragraph, however, it appears that certain gaps in, and uncertainties of, particularly the freon observational data are limiting, as is the fact that only one zonal observation section has been available. On the other hand, the fact that subjectively optimum simulations for the two horizons were obtained for the same diffusivity values provides an encouraging consistency argument. It is also to be kept in mind that, apart from the diffusivities, the model does not contain any ad hoc adjustments.

6. Discussion

We have shown that our model can adequately simulate the observed distributions of tritium, ^{3}He, and the freons on the two isopycnal horizons investigated ($\sigma_\theta = 26.5$ and 26.8). In particular, the fact that consistent agreement has been obtained between simulations and observations for these tracers that have quite different interior distributions (Figs. 8, 9) is taken as evidence that our model adequately describes the transfer of matter between the ocean surface and the upper main thermocline in the NE Atlantic on a time scale of a few years. Compared to Sarmiento's (1983b) analysis, we formulate the tracer transport explicitly, and in particular specify advection.

We find that effective outcrop boundaries for the two density horizons can consistently be identified with surface water isolines of the respective density averaged over the month of February, and our analysis places the across-boundary uncertainty of the outcrops at about ±300 km. For the $\sigma_\theta = 26.5$ horizon, our so-defined winter outcrop boundary definitely lies south of that shown in the maps of Sarmiento et al. (1982) based on winter-season averaged data. The adequacy of the winter outcrops may be surprising in view of the fact that at such a boundary the isopycnal remains buried over most of the year. It is noted, however, that flow velocities across this boundary are only of order 10^{-2} m s^{-1} (Fig. 2), so that a fluid element is carried no farther than about 300 km across within a year.

Our model fit requires an apparent diffusivity south of 29°N of $K_s = 1.7 \times 10^3$ m^2 s^{-1}. Taking a typical flow velocity as $\bar{u} = 10^{-2}$ m s^{-1} (Fig. 2), the distance $X^* = K_s/\bar{u}$ at which advection begins to dominate over alongflow mixing becomes $X^* = 170$ km. This means that transport appears to be predominantly advective. Expressed as a Peclet number, L/X^*, the numerical value for the model boxes (linear dimension $L \approx 300$ km) is about 2 and for the model area in total (dimension $\approx 8L$) about 16. Our estimated diffusivity is similar to those reported by Armi and Stommel (1983) (see section 2). The fact that in our model advection dominates over alongstream mixing means that our estimate is essentially based on effects of mixing of tracer normal to the flow trajectories, between outcrop boundary and the respective points of observation in the interior. Our estimate thus uses a very different type of information than the Armi and Stommel approach. In particular, it refers to a somewhat larger scale, i.e., length of trajectory from the outcrop versus β-triangle scale.

There is a further, again scale-related, reason that makes the agreement between the two approaches gratifying. Armi and Stommel use a flow field based on quasi-synoptic hydrographic data, whereas ours is based on historical data. Inadequacies of this flow field to represent our actual tracer flow trajectories presumably would show up disguised as mixing in our analysis. From the agreement between the two approaches we can thus conclude that our flow field is near to the actual one, i.e., the flow field based on historical hydrographic data is a valid one. In view of the variability of the flow on all scales as generally observed, or, in other words, of a scale-dependent apparent diffusivity, our finding is not at all self-evident.

The Central Water boundary near 15°W is rather well reproduced in our simulations (Figs. 8, 9). Using an across-boundary length scale of tracer decline of $L^* = 800$ km (Figs. 8, 9), the transfer velocity w_T for mixing of tracer across the boundary becomes $w_T = K_s/L^* \approx 2 \times 10^{-3}$ m s^{-1}. This value is appreciably smaller than the isopycnal velocities (Fig. 2), so that diffusive tracer loss, i.e. water exchange, across the Central Water boundary is found to be small, and the boundary is identified as an advective property. Moreover, the said mixing across the Central Water boundary, if tentatively distributed over a zonal strip 3000 km wide (15°N to 15°S, $L^+ = 3000$ km), corresponds to an exchange time scale for the strip of $L^+/w_T = 50$ years. Such a time scale appears to be compatible with the 80-year exchange time scale with Northern Hemisphere surface water implied in the construction of the southern tracer boundary condition (section 4), which boundary condition thus is consistent with only lateral transport being effective without vertical mixing having to be invoked.

We have shown that the flow trajectories entering our model area appear to be ventilated in the sense that they attain essentially surface-water tracer concentrations. It is obvious that for the $\sigma_\theta = 26.5$ horizon this arises because essentially all incoming water passes through the region of winter convection (Figs. 2a, 7), and thus has been ventilated advectively. For the deeper horizon, on the other hand, we cannot distinguish between such advective ventilation and tracer having been added by across-flow mixing, or diffusive ventilation [in our ad hoc western recirculation constructed to obtain a western tracer boundary condition (section 4) ventilation has been chosen to be diffusive only].

It is instructive to compare the total advection through our model area to upper thermocline ventilation rates obtained in the box-model approach of Sarmiento (1983b) for the entire NACW between 15°N and the winter outcrops. One finds (Table 2) that the advection through our model area accounts for only 12% (σ_θ = 26.5) and 40% (26.8), respectively, of Sarmiento's total ventilation. For the upper horizon, 18° water formation (Worthington, 1976; Jenkins, 1980) is a further ventilation mechanism. For the deeper horizon it appears that either advectively ventilating water-flow trajectories must exist to the west of 33.5°W or a considerable portion of Sarmiento's ventilation is diffusive rather than advective. Should the latter be true, Sarmiento's tritium based ventilation rates, which represent advection and mixing combined, would no longer be comparable directly with Ekman pumping rates.

Diapycnic transport has been ignored in our analysis. A consistency argument can be made, based on the fact that vertical concentration gradients for the tracers used here are very different from each other. On the other hand, an estimate based on observed vertical gradients and literature values for a typical interior-ocean diapycnal diffusivity (e.g., 2×10^{-5} m^2 s^{-1}; Armi, 1978) indicates that for our model, area, i.e., at moderate upstream distances to an outcrop, the effect of diapycnic mixing should indeed be small (see also Armi and Stommel, 1983).

A point to note is that our model/data intercomparison does not allow us to deduce information on any single one of the transport processes (i.e., isopycnal or diapycnal advection or mixing, subduction) that combine to effect the total transport, independent of the other contributing processes. This characteristic is in contrast to, for example, a flow field that can be derived as such from hydrographic data. A transient-tracer data evaluation like the present one will therefore prove consistency of a given total-transport scheme rather than give detailed information on any single process, unless additional information is introduced. This is why we chose to prescribe the isopycnal flow field. Our deduced diffusivities and outcrop boundaries will certainly depend on our chosen flow field. On the other hand, the internal consistency check provided is quite detailed, so that we still regard our deduced diffusivities, for example, as reliable estimates. A further point is that the basic asset of time dependence of oceanic transient-tracer distributions in our model evaluation as a trade-off requires time-dependent tracer boundary conditions to be established. We have resolved this difficulty by placing the model boundaries such that the tracer concentrations either are small (southern boundary) or are coinciding with or quite near to surface water concentrations (northern and western boundary, respectively). Assessability of tracer-concentration boundary conditions apparently has to be a concern in setting up a model evaluation, and it is for this reason that we have restricted our evaluation to the upper main thermocline, because for deeper horizons the upstream distances from our model area to the winter outcrops (Sarmiento et al., 1982) become large, so that the time-dependent tracer boundary conditions get out of hand.

TABLE 2. Comparison of upper main thermocline ventilation rates.

Density horizon	Volume replacement rate (10^6 m^3 s^{-1})*	
σ_θ (kg m^{-3})	NACW, 15°N to outcrop (Sarmiento, 1983b)	across 30.5°N east of 33.5°W (this work)
26.5	3.8	0.46
26.8	3.1	1.23

* Rates refer to a mean layer thickness corresponding to $\Delta\sigma = 0.1$

7. Conclusions and outlook

It is generally agreed that transient tracer data, which are to become available in increasing numbers in the foreseeable future, contain valuable information on main thermocline ventilation and interior transport. However, an accepted methodology to retrieve the contained information does not exist. The present work explores one possible line of approach, i.e., using a kinematic advection–diffusion model with prescribed advection and employing time-dependent tracer boundary conditions. We find that our model provides a consistent description of ventilation and transport, and we are able to confirm the assumed boundaries of isopycnal subduction and to estimate isopycnal diffusivities. At the same time, it becomes manifest that the tracer distributions are the integral result of, generally, several years of ocean circulation and mixing, which complicates the task of placing error bars on any isolated model transport parameter deduced. In our determination of uncertainty limits for our model diffusivities (section 5) we took the flow field and outcrop boundaries as fixed, while it would certainly be preferable to vary these as well. More work concerning this point of parameter uncertainty limits will be needed. On the other hand, the integrating characteristic of the tracer distributions may add insight to the relative importance of different transport mechanisms contributing, such as advective and diffusive ventilation (section 6).

We maintain that the validity of our conclusions strongly relies on our use of combined data for tracers that have distinctly different surface water boundary conditions and hence also interior distributions. To improve consistency further, future work would profitably include simulations for salinity as well as for oxygen (which should yield interior-ocean oxygen consumption rates). Moreover, model–data comparison in the present work was confined to observations

along one single section, but a comparison extended areally would definitely give considerably more information. Areal extension would generally have to rely on data from different cruises, so that comparisons at different points in time would have to be made. This approach would require an adequate evaluation procedure to allow an optimization using quite inhomogeneous pieces of information.

To extend our approach to deeper horizons of the main thermocline will require a northward and westward extension of our model area, in order to enable us to assess the time-dependent tracer boundary conditions (section 6). Future collection of tracer observations should be done with a view toward minimizing interpolation errors in deriving isopycnal tracer distributions. The presently available seagoing, high-precision and fast freon measurement, as well as improved tritium measurement precision, should allow considerable improvement in this respect.

One transport characteristic that appears to be assessable without too much interdependence with the other transport processes are the outcrop boundaries, which may be mapped on the basis of the ^{3}He-distribution (section 5). A dedicated ^{3}He data collection effort is suggested. It even appears that the ^{3}He age-resolution might be sufficient to allow one to study interannual variability of the outcrop boundaries in such an effort.

Acknowledgments. We are grateful to the master and crew of the F/S *Meteor* for their assistance during leg 5 of cruise no. 56, as well as to various helpers in the station work. G. Bader was responsible for the tritium measurements. We thank J. Rudolph, KFA Jülich, for providing the freon standards and calibration information, R. Schlitzer, Heidelberg, for help in the model numerics, and L. Armi, La Jolla, for a valuable comment. We have in remembrance the late W. Pohlner, Heidelberg, who developed the freon measuring system and collected the freon samples on *Meteor* cruises 56 and 57. The project was supported by the Deutsche Forschungsgemeinschaft.

REFERENCES

Armi, L., 1978: Some evidence for boundary mixing in the deep ocean. *J. Geophys. Res.*, **83,** 1971–1979.

——, and H. Stommel, 1983: Four views of a portion of the North Atlantic subtropical gyre. *J. Phys. Oceanogr.*, **11,** 828–857.

Battelle, 1976: Studie über die Auswirkungen von Fluorchlorkohlenwasserstoffverbindungen auf die Ozonschicht der Stratosphäre und die möglichen Folgen. Bericht für das Umweltbundesamt, Battelle-Institut, Frankfurt/Main.

Behringer, D. W., 1979: On computing the absolute geostrophic velocity spiral. *J. Mar. Res.*, **37,** 459–470.

——, and H. Stommel, 1980: The beta-spiral in the North Atlantic subtropical gyre. *Deep Sea Res.*, **27,** 225–238.

Benson, B. B., and D. Krause, Jr., 1980: Isotopic fractionation of helium during solution: A probe for the liquid state. *J. Solution Chem.*, **9,** 895–909.

Bullister, J. L., and R. F. Weiss, 1983: Anthropogenic chlorofluoromethanes in the Greenland and Norwegian Seas. *Science,* **221,** 265–268.

Clarke, W. B., W. J. Jenkins and Z. Top, 1976: Determination of tritium by mass spectrometric measurement of ^{3}He. *Int. J. Appl. Radiat. Isotopes,* **27,** 512–522.

Cox, M. D., and K. Bryan, 1984: A numerical model of the ventilated thermocline. *J. Phys. Oceanogr.*, **14,** 674–687.

Cunnold, D. M., R. G. Prinn, R. A. Rasmussen, P. G. Simmonds, F. N. Alyea, C. A. Cordelino, A. J. Crawford, P. J. Fraser and R. D. Rosen, 1983a: The Atmospheric Lifetime Experiment. 3: Lifetime methodology and application to three years of $CFCl_3$ data. *J. Geophys. Res.*, **88,** 8379–8400.

——, ——, ——, ——, ——, —— and ——, 1983b: The Atmospheric Lifetime Experiment. 4: Results for CF_2Cl_2 based on three years data. *J. Geophys. Res.*, **88,** 8401–8414.

Dreisigacker, E., and W. Roether, 1978: Tritium and ^{90}Sr in North Atlantic surface water. *Earth Planet. Sci. Lett.*, **38,** 301–312.

Fiadeiro, M. E., and G. Veronis, 1977: On weighted-mean schemes for the finite-difference approximation to the advection–diffusion equation. *Tellus,* **29,** 512–522.

Fuchs, G., W. Roether and P. Schlosser, 1986: Excess ^{3}He in the ocean surface layer. *J. Geophys. Res.* (submitted).

Gammon, R. H., J. Cline and D. Wisegarver, 1982: Chlorofluoromethanes in the Northeast Pacific Ocean: Measured vertical distributions and application as transient tracers of upper ocean mixing. *J. Geophys. Res.*, **87,** 9441–9454.

Gorschkov, S. G., (Ed.), 1978: *World Ocean Atlas.* Vol. 2, *Atlantic and Indian Oceans.* Pergamon, 141 plates.

Jenkins, W. J., 1980: Tritium and ^{3}He in the Sargasso Sea. *J. Mar. Res.* **38,** 533–569.

——, and W. B. Clarke, 1976: The distribution of ^{3}He in the Western Atlantic Ocean. *Deep-Sea Res.*, **23,** 481–494.

Käse, R. H., and G. Siedler, 1982: Meandering of the subtropical front southeast of the Azores. *Nature,* **300,** 245–246.

——, W. Zenk, T. B. Sanford and W. Hiller, 1985: Currents, fronts and eddy fluxes in the Canary Basin. *Progress in Oceanography,* Vol. 14, Pergamon, 231–257.

Lawson, C. L., and R. J. Hanson, 1974: *Solving Least Square Problems.* Prentice Hall, 340 pp.

Levitus, S., 1982: Climatological Atlas of the World Ocean. NOAA Prof. Paper 13, U.S. Dept. of Commerce, 173 pp.

Luyten, J. R., J. Pedlosky and H. Stommel, 1983a: The ventilated thermocline. *J. Phys. Oceanogr.*, **13,** 292–309.

——, —— and ——, 1983b: Climatic inferences from the ventilated thermocline. *Clim. Change,* **5,** 183–191.

McCartney, M. S., 1982: The subtropical recirculation of mode waters. *J. Mar. Res.*, **40**(Suppl.), 427–464.

McDowell, S., P. B. Rhines and T. Keffer, 1982: North Atlantic potential vorticity and its relation to the general circulation. *J. Phys. Oceanogr.*, **12,** 1417–1436.

Quay, P. D., M. Stuiver and W. S. Broecker, 1983: Upwelling rates for the equatorial Pacific Ocean derived from the bomb ^{14}C distribution. *J. Mar. Res.*, **41,** 769–792.

Roache, P. J., 1972: *Computational Fluid Dynamics,* Hermosa.

Robinson, M. K., R. A. Bauer and E. H. Schroeder, 1979: *Atlas of North Atlantic and Indian Ocean Monthly Mean Temperatures and Mean Salinities of the Surface Layer.* Dept. of the Navy, Washington, DC.

Sarmiento, J. L., 1983a: A simulation of bomb tritium entry into the Atlantic Ocean. *J. Phys. Oceanogr.*, **13,** 1924–1939.

——, 1983b: A tritium box model of the North Atlantic thermocline. *J. Phys. Oceanogr.*, **13,** 1269–1274.

——, and K. Bryan, 1982: An ocean transport model for the North Atlantic, *J. Geophys. Res.*, **87,** 394–408.

——, C. G. H. Rooth and W. Roether, 1982: The North Atlantic tritium distribution in 1972. *J. Geophys. Res.*, **87,** 8047–8056.

Schlitzer, R., W. Roether, P. Brewer and R. Käse, 1985: Hydrographic,

nutrient, and carbonate chemistry data, *Meteor* cruise no. 56 leg 5, NE Atlantic, Mar.–Apr. 1981. Unpublished manuscript.

Siedler, G., and L. Stramma, 1983: The applicability of the *T/S* method to geopotential anomaly computations in the Northeast Atlantic. *Oceanol. Acta,* **6**(2), 167–172.

——, W. Zenk and W. J. Emery, 1985: Strong-current events related to a subtropical front in the Northeast Atlantic. *J. Phys. Oceanogr.,* **15,** 885–897.

Stramma, L., 1984: Geostrophic transports in the warm water sphere of the eastern subtropical North Atlantic. *J. Mar. Res.,* **42**(3), 537–558.

Taylor, C. B., and W. Roether, 1982: A uniform scale for reporting low-level tritium measurements in water. *Int. J. Appl. Radiat. Isotopes,* **33,** 377–382.

U.S. Naval Oceanographic Office, 1967: *Oceanographic Atlas of the North Atlantic Ocean, Sec. II, Physical Properties.* Washington, DC, Publ. No. 700, 308 pp.

Warner, M. J., and R. F. Weiss, 1985: Solubility of chlorofluorocarbons 11 and 12 in water and seawater. *Deep-Sea Res.,* **32,** 1485–1497.

Weiss, R. F., 1968: Piggy back samplers for dissolved gas studies on sealed water samples. *Deep Sea Res.,* **15,** 695–699.

Weiss, W., and W. Roether, 1980: The rates of tritium input to the world oceans. *Earth Planet. Sci. Lett.,* **49,** 435–446.

——, —— and G. Bader, 1976: Determination of blanks in low-level tritium measurement. *Int. J. Appl. Radiat. Isotopes,* **27,** 217–225.

——, —— and E. Dreisigacker, 1979: Tritium in the North Atlantic Ocean: Inventory, input and transfer into deep water. *Behaviour of Tritium in the Environment,* IAEA, Vienna, 315–336.

Wisegarver, D. P., and J. D. Cline, 1985: Solubility of trichlorofluoromethane (F-11) and dichlorodifluoromethane (F-12) in seawater and its relationship to surface concentrations in the North Pacific. *Deep-Sea Res.,* **32,** 97–106.

Worthington, L. V., 1976: *On the North Atlantic Circulation. The Johns Hopkins Oceanographic Studies,* No. 6, Johns Hopkins University Press, 110 pp.